

Solar variability in the Mg II h and k lines

K. SOWMYA,^{1,2} M. SNOW,^{3,4,5} A. I. SHAPIRO,^{2,1} N. A. KRIVOVA,¹ T. CHATZISTERGOS,¹ AND S. K. SOLANKI¹

¹*Max-Planck-Institut für Sonnensystemforschung, Justus-von-Liebig-Weg 3, 37077 Göttingen, Germany*

²*Institute of Physics, University of Graz, Universitätsplatz 5, 8010 Graz, Austria*

³*Laboratory for Atmospheric and Space Physics, University of Colorado Boulder, 1234 Innovation Dr., Boulder CO 80303, USA*

⁴*South African National Space Agency, Hospital Street, Hermanus 7200, South Africa*

⁵*Department of Physics and Astronomy, University of the Western Cape, Robert Sobukwe Road, Bellville 7535, South Africa*

ABSTRACT

Solar irradiance and its variations in the ultraviolet (UV) control the photochemistry in Earth's atmosphere and influence Earth's climate. The variability of Mg II h and k core-to-wing ratio, also known as the Mg II index, is highly correlated with the solar UV irradiance variability. Because of this, Mg II index is routinely used as a proxy for solar UV irradiance variability, which can help to get insights into the influence of solar UV irradiance variability on Earth's climate. Measurements of the Mg II index, however, have only been carried out since 1978 and do not cover the climate relevant timescales longer than a few decades. Here we present a model to calculate the Mg II index and its variability based on the well-established SATIRE (Spectral And Total Irradiance REconstruction) model. We demonstrate that our model calculations yield an excellent agreement with the observed Mg II index variations, both on the solar activity cycle and on the solar rotation timescales. Using this model, we synthesize Mg II index timeseries on climate relevant timescales of decades and longer. Here we present the timeseries of the Mg II index spanning nearly three centuries.

Keywords: Solar activity (1475) – Solar ultraviolet emission(1533) – Solar chromosphere(1479) – Plages (1240) – Solar transition region(1532)

1. INTRODUCTION

The solar radiation, which is the main source of energy input to the Earth, varies at all measurable timescales and wavelengths. The constantly evolving solar surface magnetic fields are established to be the main drivers of such variations on timescales longer than a day (Krivova et al. 2003; Yeo et al. 2017; Shapiro et al. 2017). These evolving surface magnetic fields extend to the chromosphere, where the bulk of the ultraviolet (UV) radiation forms. There they lead to local brightenings that regulate the solar UV output. Variations in the solar UV radiation influence Earth's climate via the so called top-down mechanism (see e.g. reviews by Gray et al. 2010; Ermolli et al. 2013; Solanki et al. 2013). An accurate reconstruction of the solar UV irradiance and its variability is therefore crucial for understanding the role of solar variability in causing natural climate change.

Due to the lack of long and stable, directly measured timeseries of solar UV irradiance, studies of the impact of solar UV irradiance on Earth's climate often rely on proxies. The most important of solar UV irradiance proxies is the Mg II core-to-wing ratio that is also often called the Mg II index (Heath & Schlesinger 1986, see also Snow et al. 2019) based on the Mg II h and k emission around 280 nm. Because it is a ratio of fluxes (at nearby wavelengths), it is less prone to instrumental effects than the fluxes themselves. Further, the Mg II index is known to be strongly correlated with the solar UV irradiance below 400 nm (e.g. Heath & Schlesinger 1986; Viereck & Puga 1999; Viereck et al. 2001) and it has even been used as a direct input in Earth's atmosphere modeling (e.g. Thuillier et al. 2012, see also Thuillier & Bruinsma 2001; Bruinsma et al. 2003). However, the measurements of this index span only a few decades (starting

from 1978) and therefore different approaches have been developed to create a continuous and longer timeseries of Mg II index which is required for Earth’s atmosphere and climate studies.

A number of reconstructions of Mg II index data are based on the observed correlation between Mg II index and other solar indices. For example, [Deland & Cebula \(1993\)](#) used the correlation between Mg II index and the solar radio flux at 10.7 cm to create a composite of Mg II index covering the period 1978-1992. By designing a model for the Mg II index data from 10.7 cm flux using neural networks, [Tebabal et al. \(2017\)](#) extrapolated the Mg II index to 1947. Recently, [Roy et al. \(2021\)](#) exploited the correlation between Mg II index and 10.7 cm to fill gaps in existing Mg II index observations. Further, Mg II h and k emission shows a strong correlation with Ca II H and K emission ([Donnelly et al. 1994](#)) since they form around similar heights in the solar atmosphere and trace the same plasma ([Vernazza et al. 1981](#), see also [Linsky 2017](#)). Based on this property, [Morrill et al. \(2011\)](#) developed an approach using Ca II K images from Mt. Wilson observatory to estimate Mg II index between 1961 and 1981. Using the correlations found between the Mg II index and neutron-monitor data and applying them to the cosmogenic isotope data, [Thuillier et al. \(2012\)](#) reconstructed Mg II index back to the Maunder minimum period.

Another class of approaches is based on combining synthetic spectra of magnetic features and quiet-Sun with observed distribution of magnetic features on the solar disk. For example, [Criscuoli et al. \(2018\)](#) used synthetic spectra and area coverages of the magnetic features determined using Ca II K and photospheric red continua full disk images from several ground-based telescopes to reconstruct Mg II index back to 1989. It was later extended further back to 1749 by [Berrilli et al. \(2020\)](#).

Here we take a similar approach but build on the success of the SATIRE-S (Spectral And Total Irradiance REconstruction for the Satellite era) model which has a very comprehensive methodology for defining the disk distribution of magnetic features. It directly uses magnetic field information from observed full disk solar magnetograms, and intensity images to determine the area coverage of magnetic features ([Fligge et al. 2000](#); [Krivova et al. 2003, 2011](#); [Yeo et al. 2014](#)). This allowed SATIRE-S model to yield a remarkable agreement with observations of total and spectral solar irradiance.

Traditionally SATIRE-S model employed spectra from [Unruh et al. \(1999\)](#) synthesized in local thermodynamic equilibrium (LTE) using 1D atmospheres without a chromosphere. This is sufficient for calculating solar irradiance longward of 300 nm but requires an empirical correction below it ([Krivova et al. 2006](#); [Yeo et al. 2014](#)). Recently [Tagirov et al. \(2019\)](#) included non-LTE modelling into SATIRE-S and reconstructed solar UV irradiance (with 1 nm spectral resolution, not resolving strong spectral lines such as Ca II H and K, Mg II h and k, and hydrogen lines) circumventing the need for the empirical correction. Later [Sowmya et al. \(2021\)](#) used SATIRE-based approach to model the variability of solar Ca II H and K lines. Here we focus on modelling the high resolution spectral profile of Mg II h and k lines. Namely, we take SATIRE-S distributions of magnetic features and combine them with Mg II h and k spectra of quiet-Sun and magnetic features. These spectra are obtained using 1D semi-empirical solar atmospheric models and include a proper treatment of the physical mechanisms governing the properties of Mg II h and k lines. In particular, they account for non-LTE effects and partial frequency redistribution in line cores.

Our approach is described in Section 2. In Section 3.1, we show that the synthetic Mg II index values are in excellent agreement with the observations from SOLar-STellar Irradiance Comparison Experiment (SOLSTICE) on the Solar Radiation and Climate Experiment (SORCE; [Rottman 2005](#)). We further demonstrate that our approach reproduces the observed variations of Mg II index both on the solar rotation and activity cycle timescales. The extension of the Mg II index timeseries to 1745 is described in Section 3.2 and conclusions are presented in Section 4.

2. METHODS

Our SATIRE-S based model attributes irradiance changes on timescales longer than a day to the changes in the surface magnetic field, which manifests as dark sunspots and bright faculae (although the chromospheric counterparts of faculae are called plages, we refer to both faculae and plages collectively as ‘faculae’ throughout the paper for simplicity). The disk integrated solar flux F at a given time t and wavelength λ is therefore computed by combining the area coverages of quiet-Sun (regions free of the magnetic features), sunspots and faculae with their corresponding brightness. However, we neglect sunspots following the finding that solar UV emission is dominated by contribution from faculae ([Lean & Repoff 1987](#); [Lean et al. 1997](#); [Unruh et al. 2008](#); [Penza et al. 2023](#); [Sowmya et al. 2023](#)). The quiet-Sun and facular fluxes are computed by decomposing the solar disk into l concentric rings whose positions are defined by μ_l (cosine of the heliocentric angle θ). Namely,

$$F(t, \lambda) = \sum_l I_q(\lambda, \mu_l) \Delta\Omega_l + \sum_l \alpha_{fl}(t) [I_f(\lambda, \mu_l) - I_q(\lambda, \mu_l)] \Delta\Omega_l, \quad (1)$$

where $\alpha_{fl}(t)$ are the time dependent fractional area coverages of faculae in the l th ring which subtends a solid angle of $\Delta\Omega_l$ at a distance of 1 AU from the Sun. $I_q(\lambda, \mu_l)$ and $I_f(\lambda, \mu_l)$ are the specific intensities of quiet-Sun and faculae, respectively.

The specific intensities in Equation (1) are computed using the RH code (Uitenbroek 2001) by including the non-LTE and partial frequency redistribution effects which are essential to explain the shapes of the Mg II h and k lines (see e.g. Uitenbroek 1997). A 22-level configuration for the Mg atom provided in the RH code is used (MgI.b+MgII.atom). The atmospheric structure of the quiet-Sun is represented by model C while that of faculae by model P of Fontenla et al. (1999). Background lines in the wavelength window between 274 and 286 nm are included from Kurucz’s line list¹ to determine background line opacity and emissivity in LTE conditions.

To validate the modeled spectra synthesized using the approach above, we use level 2 quiet-Sun disk center raster observations from Interface Region Imaging Spectrograph (IRIS; De Pontieu et al. 2014) and Total and Spectral Solar Irradiance Sensor-1 (TSIS-1) hybrid solar reference spectrum from Coddington et al. (2023). IRIS observations used here were recorded on 05 October 2022 between 04:10:19 UT and 04:28:24 UT, and cover a field of view of 127”x119”. IRIS radiometric calibration procedure on SSW IDL was used to convert the data number units to intensity in physical units ($\text{W m}^{-2} \text{Sr}^{-1} \text{nm}^{-1}$).

Our synthetic quiet-Sun spectrum reproduces the line core and near-wing features observed by IRIS remarkably well as shown in Figure 1a (see also inset). However, the synthetic spectrum overestimates the intensities in the far-wings of the Mg II lines (compare spectra shown in blue and black in Figure 1a). This is due to the well known missing opacity issue in the UV arising from incomplete spectral line lists (Kurucz 2009). To correct for these missing spectral lines, we followed the H-minus opacity correction approach introduced by Bruls et al. (1992). The disk-center spectrum obtained after the opacity correction is shown in red in Figure 1a. For simplicity, the correction factors are assumed to be independent of μ_l . Our synthetic disk-integrated spectral flux, computed under such an assumption, results in a good agreement with the TSIS-1 spectrum, as can be seen in Figure 1b. We note that line broadening by macroturbulent velocity fields is taken into account by convolving the Mg II line cores with a Gaussian profile having FWHM of 200 mÅ (corresponding to a velocity of $\sim 21 \text{ km s}^{-1}$). Spectral regions outside the line cores, which form lower in the atmosphere than the line cores (mainly the photospheric spectral lines in the Mg II line wings), are convolved with a Gaussian profile of 100 mÅ (corresponding to a velocity of $\sim 10 \text{ km s}^{-1}$). These velocities, required to reproduce the observed line widths, are consistent with the plasma velocity amplitudes in the formation layers of Mg II lines, as determined from 3D magnetohydrodynamic simulations (Ondratschek et al. 2024).

The fractional area coverages of faculae in Equation (1), for the time period 1999–present, are taken from Yeo et al. (2014) and extended further to the present time with their method (Sowmya et al. 2021, Yeo, K. L., private communication). The method of Yeo et al. (2014) is based on the photospheric full disk continuum intensity and magnetogram images from ground- and space-based observations. Although the facular area coverages recovered with their approach goes back to 1975 (see Figure 5), we limit it to 1999 (a) due to the gaps in the facular area coverages for the solar cycles before 1999 and (b) due to the availability of better quality space-based solar continuum intensity and magnetogram images starting from 1999 (basically uninterrupted after the SOHO ”vacation”). For the reconstruction of Mg II indices in the interval 1745–1998, the fractional area coverages of faculae from Wu et al. (2018, see also Krivova et al. 2007) are used. Wu et al. (2018) reconstructed the past evolution of the solar magnetic flux from the sunspot number, which is the only available direct solar activity metric before the late 19th century, by solving a set of coupled ordinary differential equations (Solanki et al. 2000, 2002; Vieira & Solanki 2010). The magnetic flux was then converted into fractional area coverages of the magnetic features as described by Krivova et al. (2006).

For calculating the Mg II index, we follow a new definition presented in Snow et al. (2019) based on SORCE/SOLSTICE spectra at 0.1 nm resolution. This revised definition uses weighted sums of fluxes at specific spectral regions in core and wing (shown as gray shaded b, h, k, and r regions in Figure 1b) instead of using fluxes at 7 specific wavelength positions as in the traditional definition (Heath & Schlesinger 1986). We refer to Snow et al. (2019) for a detailed discussion of the need for this new algorithm to calculate Mg II index. To be consistent with

¹ <http://kurucz.harvard.edu/linelists.html>

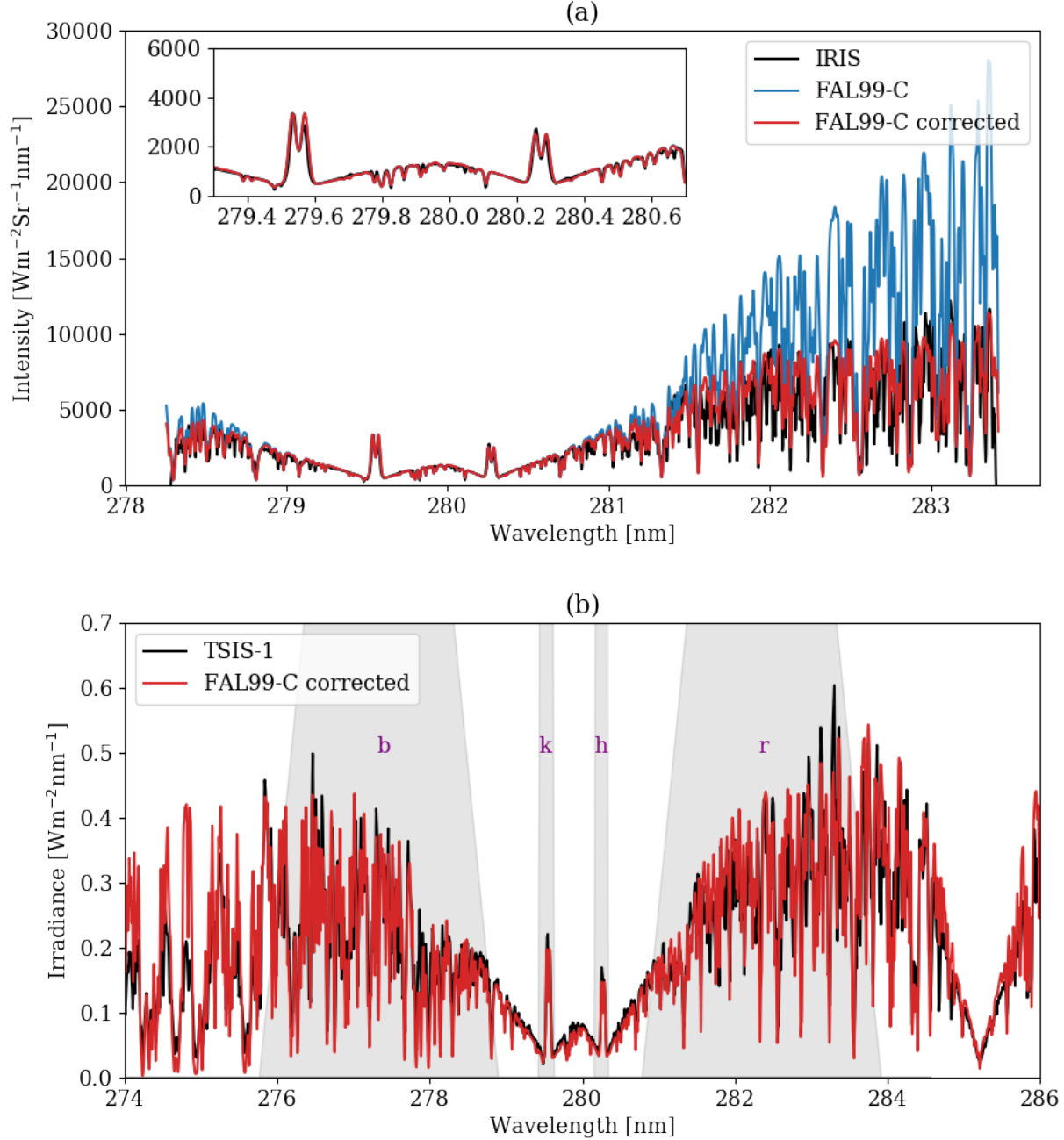


Figure 1. Comparison between observed and modeled spectra. Panel (a): disk-center quiet-Sun spectrum observed by IRIS (black), FAL99-C spectrum before (blue) and after (red) applying the H-minus opacity corrections in spectral synthesis. Panel (b): quiet-Sun irradiance spectrum from Coddington et al. (2023, black) and FAL99-C after opacity corrections (red). Gray shaded areas marked b, k, h, and r are the masks used to determine the Mg II index. See Section 2 for details.

definition of Snow et al. (2019), we smooth the synthetic spectra to a spectral resolution of 0.1 nm (Snow et al. 2005) and resample them to the SORCE/SOLSTICE wavelength grid with a spacing of 0.02 nm. We then compute the Mg II index and its time variations using:

$$\text{Mg II index} = \frac{C_k + C_h}{W_b + W_r}, \quad (2)$$

where C_k and C_h are the weighted sums of fluxes in the cores while W_b and W_r are the weighted sums of fluxes in the wings. They are obtained as

$$\frac{\sum_{b,h,k,r} x_\lambda * F(t, \lambda)}{\sum_{b,h,k,r} x_\lambda},$$

where x_λ are the wavelength-dependent weights from [Snow et al. \(2019\)](#). While calculating the flux in the line core regions, we multiply the facular area coverages by a constant factor following [Sowmya et al. \(2021\)](#). This accounts for the expansion of flux tubes forming faculae as they rise to the chromosphere where the Mg II h and k line cores form. By carrying out a linear regression of the calculated Mg II index values with those observed, we determine the value of this expansion factor to be 3.0. This value of the expansion factor gives a regression slope very close to unity. It is reassuring that this value is close to the expansion factor of 2.9 used by [Sowmya et al. \(2023\)](#) to model Ca II H and K emission, since the Mg II h and k emission forms around similar heights.

3. RESULTS

3.1. Comparison with *SORCE/SOLSTICE* measurements

To test the performance of our model, we compute Mg II indices using the facular area coverages obtained following [Yeo et al. \(2014\)](#) and compare them with *SORCE/SOLSTICE* Mg II index measurements from [Snow et al. \(2019\)](#). [Figure 2a](#) shows a comparison of the timeseries of daily Mg II indices from our model with the data while [Figure 2b](#) shows the correlation between the two records on common available days. The high correlation between the observations and the model (0.98) is reassuring.

For a better assessment of the agreement between our calculations and observations we separately consider Mg II index variability on the activity cycle and on the solar rotation timescales. Our calculations reproduce variability on the activity timescale reasonably well. This is showcased in [Figure 3](#) where we plot 81-day (corresponding to three solar rotations) running averages of observed and modelled Mg II indices. However, [Figure 3](#) also points to some systematic deviations. The model values are consistently higher than what is observed prior to 2010. Between 2010 and 2016, the model values are lower than observed while beyond 2016, the model values switch again to being slightly higher than observations. These deviations could either reflect inaccuracies in the model (for example, in facular area determinations or in spectral synthesis) or instrumental effects.

The deviations could possibly have an instrumental origin, as the *SOLSTICE* data might be affected by calibration issues over some periods of time. [Woods et al. \(2021\)](#) describe the operational challenges to the *SORCE* spacecraft throughout the mission. The primary issues affecting the Mg II measurements are the loss of stellar calibration observations from 2008 onwards and the two extended spacecraft safe holds in 2011 and 2013 due to degradation of the spacecraft battery system ([Snow et al. 2022](#)). Significant calibration corrections needed to be applied after the 2013 safe hold which lasted for eight months until early 2014. These wavelength-dependent calibration corrections may indeed have produced a drift in the Mg II index.

Rotational variability is obtained by subtracting the 81-day running averages from the daily Mg II index timeseries. [Figure 4](#) compares the modeled variability over the 27-day rotation period with observed variations at three time intervals indicated by the red shaded regions in [Figure 3](#). These intervals correspond to the time when modeled Mg II index values on activity cycle timescale are higher than values observed by *SORCE/SOLSTICE* ([Figure 4a](#)), to the cycle minimum period when the two are comparable ([Figure 4b](#)), and to the time when model values are lower than observations ([Figure 4c](#)). The agreement between the model and observations is remarkable irrespective of the level and phase of the activity cycle.

3.2. Mg II index composite timeseries

Since the calculated timeseries presented in [Section 3.1](#) based on [Yeo et al. \(2014\)](#) can only be extended as far back as 1975, we reconstruct Mg II indices back to 1745 using the facular areas from [Wu et al. \(2018\)](#). A glimpse of this reconstructed Mg II index timeseries, covering the period between 1975 and the present, is shown by the red dashed lines in [Figure 5a](#). By design (essentially owing to the fact that only sunspot observations are available over such long periods of time), these reconstructed facular coverages are only accurate on time scales longer than the solar rotation. Therefore, we use 81-day running averages of the modeled Mg II index values to prepare the composite timeseries.

For comparison, in [Figure 5a](#) we also show the timeseries from [Section 3.1](#) (red solid line) which gives an excellent agreement with the observations (shown in black). This figure implies that although the cycle amplitudes are comparable in the two versions, the Mg II index reconstructed from the [Wu et al. \(2018\)](#) facular coverages is generally

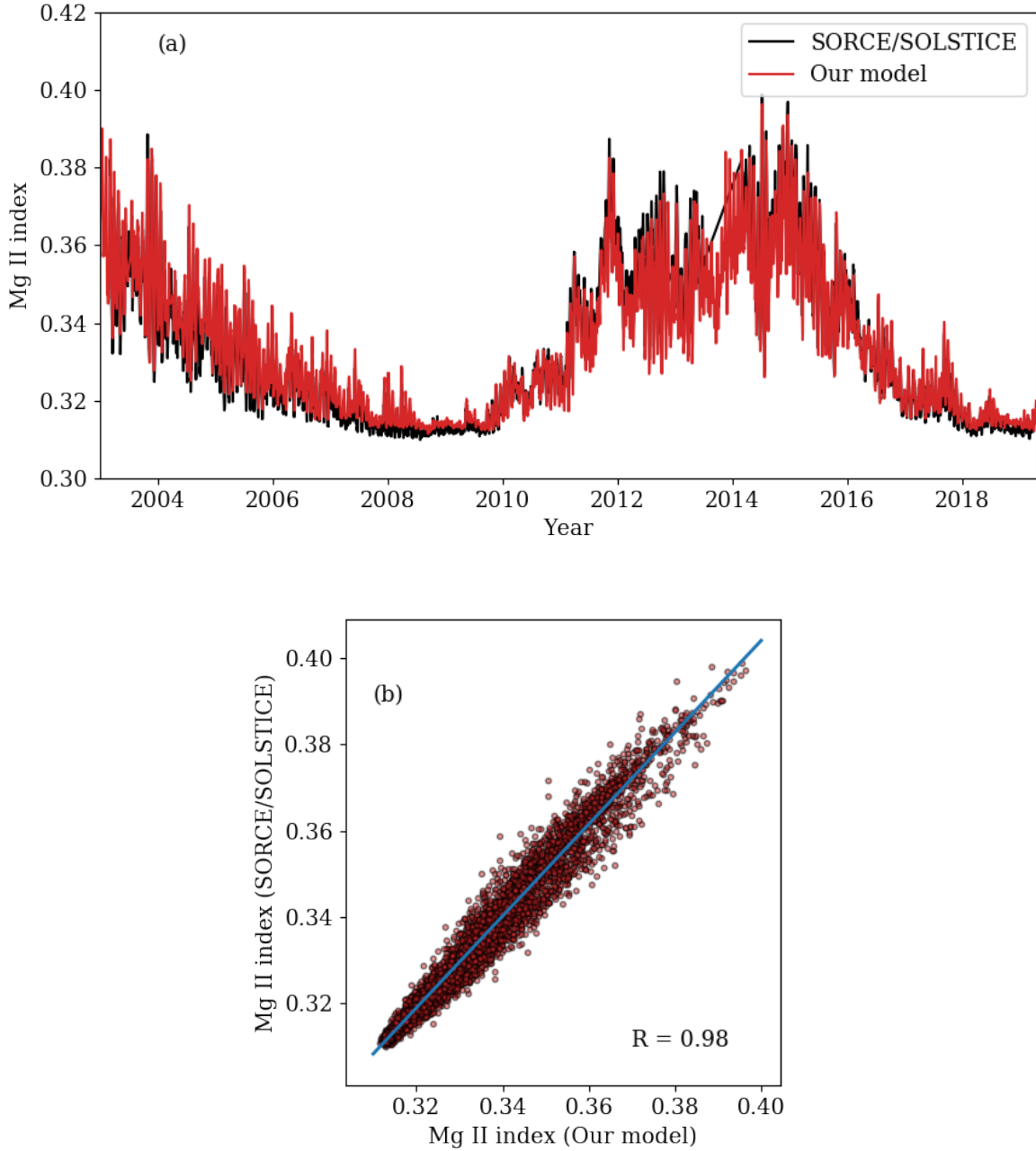


Figure 2. Comparison between observed and modeled Mg II indices. Panel (a): daily values from SORCE/SOLSTICE (black) and our model (red). Panel (b): linear regression of the observed and modeled Mg II indices (performed by choosing only those days for which both observed and modeled data are available i.e. only common available days). The Pearson linear correlation coefficient $R = 0.98$.

lower than that based on the coverages from Yeo et al. (2014). Since facular coverages of Yeo et al. (2014) are directly based on observed magnetograms, they are more accurate than coverages from Wu et al. (2018) that are based on sunspot number counts and model of the solar magnetic field evolution. Therefore, we carry out a linear regression and calibrate the Mg II index timeseries obtained using facular areas from Wu et al. (2018) to the same scale as the Mg II index timeseries obtained using faculae areas based on Yeo et al. (2014) as

$$\text{Mg II}_{\text{Yeo et al. (2014)}} = 1.113 * \text{Mg II}_{\text{Wu et al. (2018)}} - 0.028. \quad (3)$$

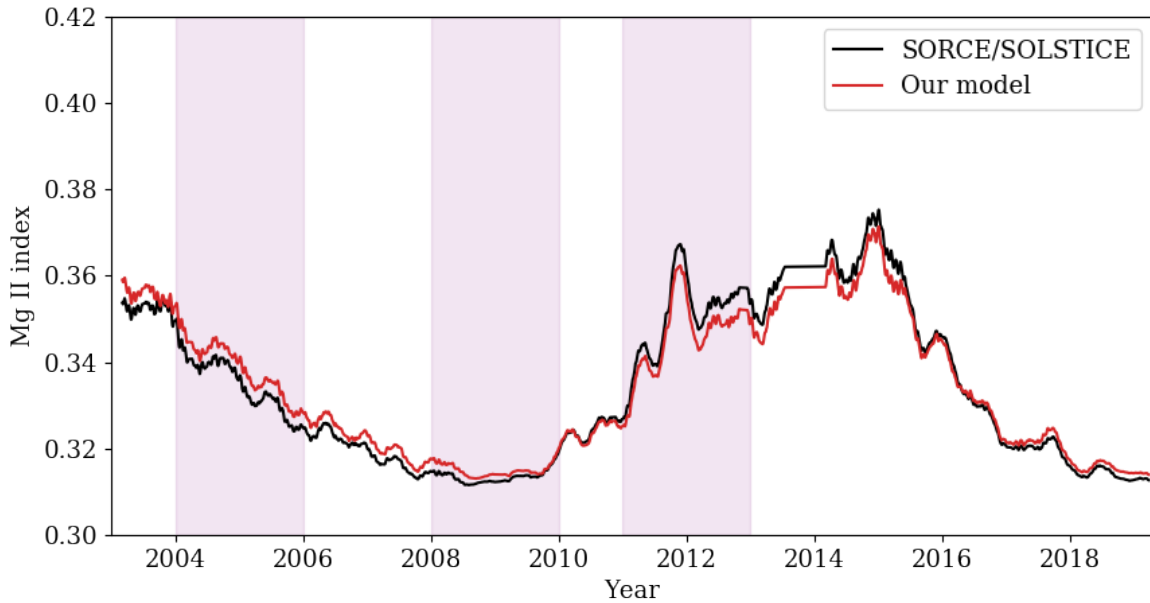


Figure 3. Solar cycle variability of the Mg II index, calculated by taking 81-day running averages of the Mg II indices shown in Figure 2. Observations from SORCE/SOLSTICE are shown in black and model calculations are shown in red. The shaded regions mark the intervals chosen to investigate rotational variability (see Figure 4).

The result of this calibration is shown in Figure 5b. Finally, we obtain the Mg II index composite shown in Figure 6, covering nearly three centuries. This composite is a combination of the Wu et al. (2018) based timeseries for the period 1745–1998 and the Yeo et al. (2014) based timeseries after 1998.

4. CONCLUSIONS

The Mg II index is a widely used proxy for solar UV irradiance. In this work, we have presented a model for the Mg II index variability based on the SATIRE approach. Specifically, we combined partial redistribution non-LTE radiative transfer computations of the Mg II line profiles in standard model atmosphere with magnetic filling factors taken from magnetograms. We have demonstrated that our model successfully reproduces the Mg II index variability observed by SORCE/SOLSTICE on activity cycle and on solar rotation timescales. We have created timeseries of the Mg II index spanning nearly three centuries, which is made available as a supplementary material. This timeseries could be used as an input for modeling the impact of solar variability, in particular in the UV, on Earth’s climate. Furthermore, this timeseries could serve as an input in planetary atmosphere modeling approaches which use proxies of solar UV irradiance (e.g. Lundin et al. 2013; Peter et al. 2014, see also de Oliveira et al. 2024).

We thank the anonymous referee for their helpful comments. This study has made use of SAO/NASA Astrophysics Data System’s bibliographic services and the open source Python package Matplotlib (Hunter 2007). We acknowledge support from the European Research Council (ERC) under the European Union’s Horizon 2020 research and innovation program (grant No. 101118581 and No. 101097844) and the South African National Research Foundation (Grant Number 132800).

REFERENCES

- Berrilli, F., Criscuoli, S., Penza, V., & Lovric, M. 2020, *SoPh*, 295, 38, doi: [10.1007/s11207-020-01603-5](https://doi.org/10.1007/s11207-020-01603-5)
- Bruinsma, S., Thuillier, G., & Barlier, F. 2003, *Journal of Atmospheric and Solar-Terrestrial Physics*, 65, 1053, doi: [10.1016/S1364-6826\(03\)00137-8](https://doi.org/10.1016/S1364-6826(03)00137-8)
- Bruls, J. H. M. J., Rutten, R. J., & Shchukina, N. G. 1992, *A&A*, 265, 237
- Coddington, O. M., Richard, E. C., Harber, D., et al. 2023, *Earth and Space Science*, 10, e2022EA002637, doi: [10.1029/2022EA002637](https://doi.org/10.1029/2022EA002637)

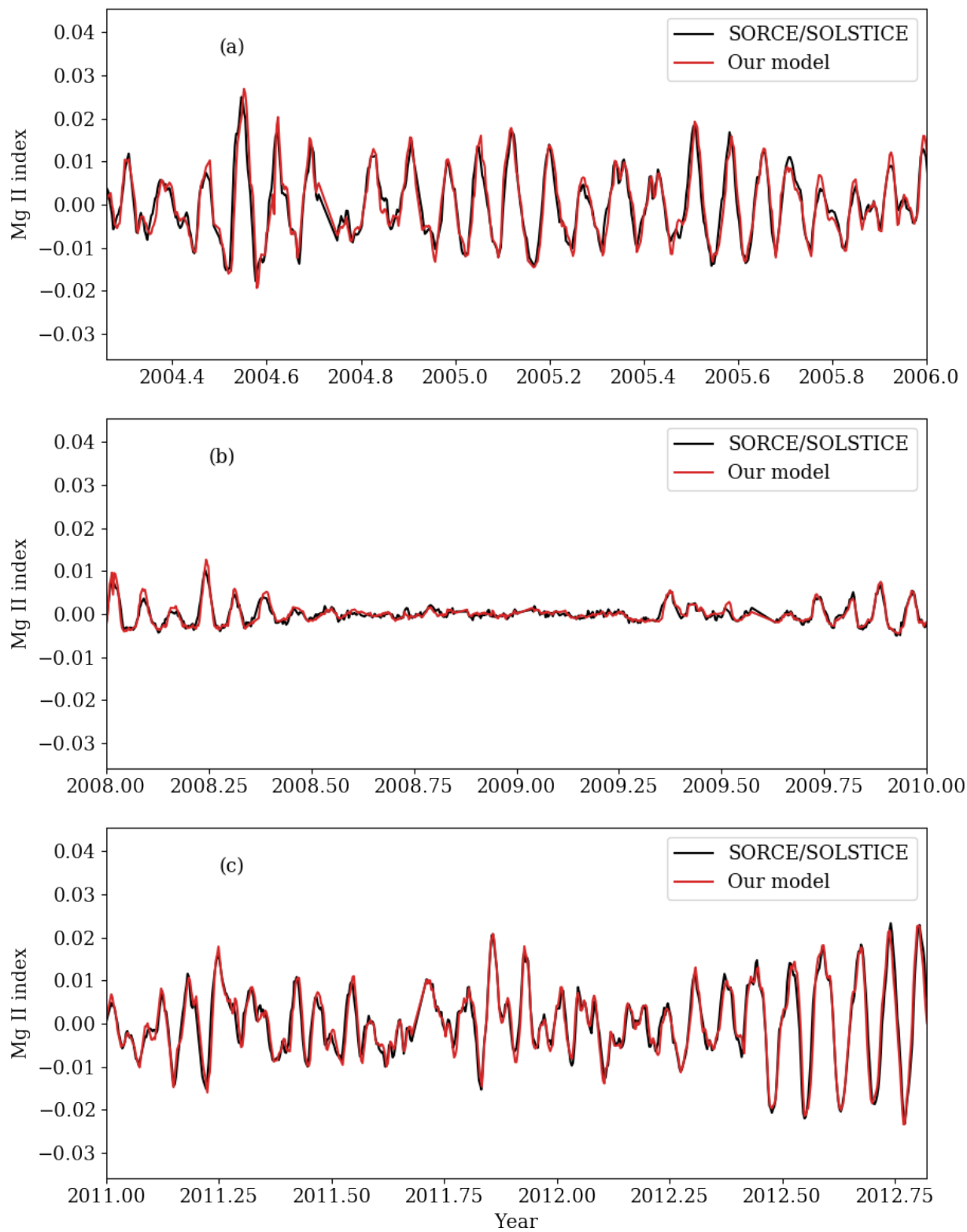


Figure 4. Rotational variability of the Mg II index during the declining phase of cycle 23 (panel a), during activity minimum of cycles 23–24 (panel b), and close to the cycle 24 maximum (panel c). Model calculations are shown in red while observations are in black.

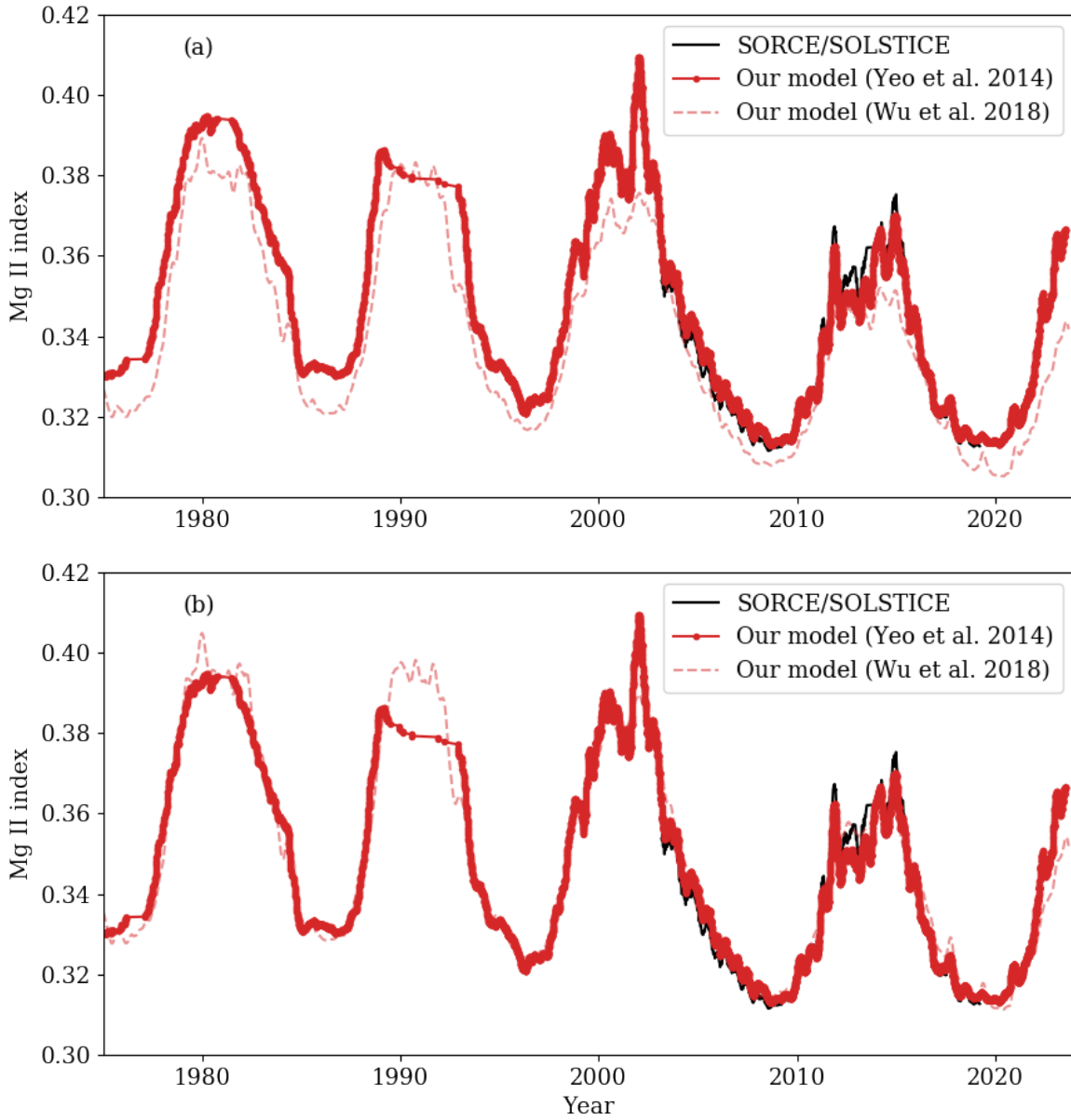


Figure 5. Comparison between 81-day running averages of the Mg II indices calculated using two different facular area inputs. Red dashed line: with facular area coverages based on [Wu et al. \(2018\)](#), red solid line: with facular area coverages based on [Yeo et al. \(2014\)](#). For completeness, the observations from SORCE/SOLSTICE are also shown (black). Panel (a) shows the two original calculated timeseries while panel (b) shows the timeseries after offset correction. See Section 3.2 for details.

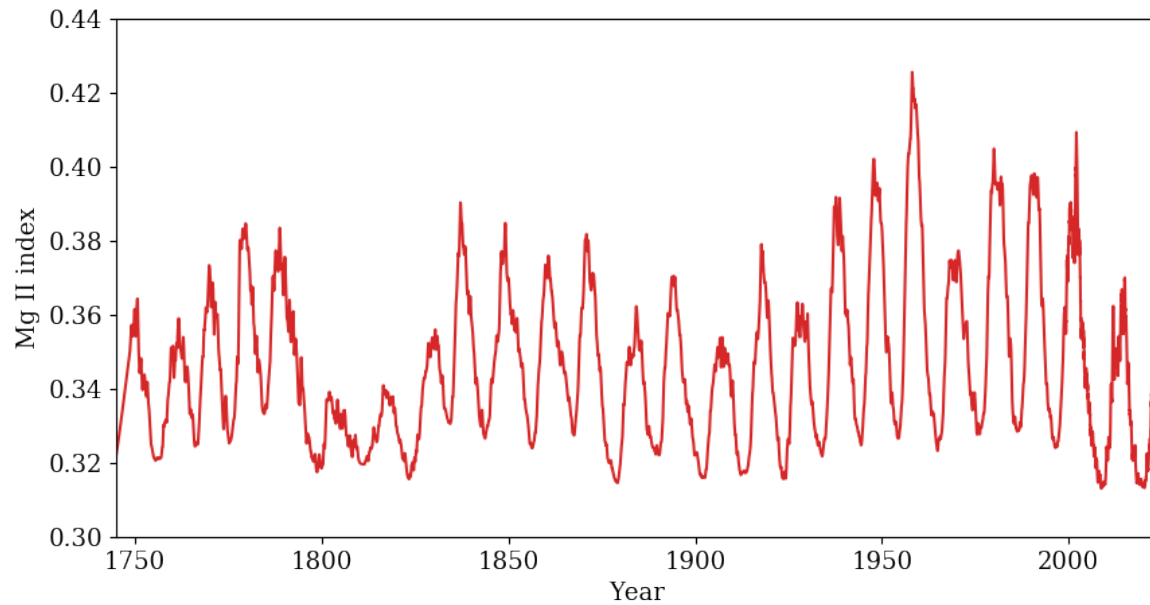


Figure 6. Mg II index composite created using the two synthetic timeseries shown in Figure 5b. For the interval 1745–1998, the facular area input from Wu et al. (2018) is used, while during 1999–present the facular area coverages based on Yeo et al. (2014) are used. The data used for this figure is available for download as supplementary material.

- Criscuoli, S., Penza, V., Lovric, M., & Berrilli, F. 2018, *ApJ*, 865, 22, doi: [10.3847/1538-4357/aad809](https://doi.org/10.3847/1538-4357/aad809)
- de Oliveira, I., Sowmya, K., Nèmec, N. E., & Shapiro, A. I. 2024, *Journal of Geophysical Research (Space Physics)*, 129, e2024JA032601, doi: [10.1029/2024JA032601](https://doi.org/10.1029/2024JA032601)
- De Pontieu, B., Title, A. M., Lemen, J. R., et al. 2014, *SoPh*, 289, 2733, doi: [10.1007/s11207-014-0485-y](https://doi.org/10.1007/s11207-014-0485-y)
- Deland, M. T., & Cebula, R. P. 1993, *J. Geophys. Res.*, 98, 12,809, doi: [10.1029/93JD00421](https://doi.org/10.1029/93JD00421)
- Donnelly, R. F., White, O. R., & Livingston, W. C. 1994, *SoPh*, 152, 69, doi: [10.1007/BF01473185](https://doi.org/10.1007/BF01473185)
- Ermolli, I., Matthes, K., Dudok de Wit, T., et al. 2013, *Atmospheric Chemistry & Physics*, 13, 3945, doi: [10.5194/acp-13-3945-2013](https://doi.org/10.5194/acp-13-3945-2013)
- Fligge, M., Solanki, S. K., & Unruh, Y. C. 2000, *A&A*, 353, 380
- Fontenla, J., White, O. R., Fox, P. A., Avrett, E. H., & Kurucz, R. L. 1999, *ApJ*, 518, 480, doi: [10.1086/307258](https://doi.org/10.1086/307258)
- Gray, L. J., Beer, J., Geller, M., et al. 2010, *Reviews of Geophysics*, 48, RG4001, doi: [10.1029/2009RG000282](https://doi.org/10.1029/2009RG000282)
- Heath, D. F., & Schlesinger, B. M. 1986, *J. Geophys. Res.*, 91, 8672, doi: [10.1029/JD091iD08p08672](https://doi.org/10.1029/JD091iD08p08672)
- Hunter, J. D. 2007, *Computing in Science & Engineering*, 9, 90, doi: [10.1109/MCSE.2007.55](https://doi.org/10.1109/MCSE.2007.55)
- Krivova, N. A., Balmaceda, L., & Solanki, S. K. 2007, *A&A*, 467, 335, doi: [10.1051/0004-6361:20066725](https://doi.org/10.1051/0004-6361:20066725)
- Krivova, N. A., Solanki, S. K., Fligge, M., & Unruh, Y. C. 2003, *A&A*, 399, L1, doi: [10.1051/0004-6361:20030029](https://doi.org/10.1051/0004-6361:20030029)
- Krivova, N. A., Solanki, S. K., & Floyd, L. 2006, *A&A*, 452, 631, doi: [10.1051/0004-6361:20064809](https://doi.org/10.1051/0004-6361:20064809)
- Krivova, N. A., Solanki, S. K., & Unruh, Y. C. 2011, *Journal of Atmospheric and Solar-Terrestrial Physics*, 73, 223, doi: [10.1016/j.jastp.2009.11.013](https://doi.org/10.1016/j.jastp.2009.11.013)
- Kurucz, R. L. 2009, in *American Institute of Physics Conference Series*, Vol. 1171, American Institute of Physics Conference Series, ed. I. Hubeny, J. M. Stone, K. MacGregor, & K. Werner, 43–51, doi: [10.1063/1.3250087](https://doi.org/10.1063/1.3250087)
- Lean, J. L., & Repoff, T. P. 1987, *J. Geophys. Res.*, 92, 5555, doi: [10.1029/JD092iD05p05555](https://doi.org/10.1029/JD092iD05p05555)
- Lean, J. L., Rottman, G. J., Kyle, H. L., et al. 1997, *J. Geophys. Res.*, 102, 29939, doi: [10.1029/97JD02092](https://doi.org/10.1029/97JD02092)
- Linsky, J. L. 2017, *ARA&A*, 55, 159, doi: [10.1146/annurev-astro-091916-055327](https://doi.org/10.1146/annurev-astro-091916-055327)
- Lundin, R., Barabash, S., Holmström, M., et al. 2013, *Geophys. Res. Lett.*, 40, 6028, doi: [10.1002/2013GL058154](https://doi.org/10.1002/2013GL058154)
- Morrill, J. S., Floyd, L., Ulrich, R., Weaver, S., & McMullin, D. 2011, *SoPh*, 270, 109, doi: [10.1007/s11207-011-9724-7](https://doi.org/10.1007/s11207-011-9724-7)
- Ondratschek, P., Przybylski, D., Smitha, H. N., et al. 2024, *A&A*, 692, A6, doi: [10.1051/0004-6361/202450788](https://doi.org/10.1051/0004-6361/202450788)

- Penza, V., Bertello, L., Cantoresi, M., Criscuoli, S., & Berrilli, F. 2023, *Rendiconti Lincei. Scienze Fisiche e Naturali*, 34, 663, doi: [10.1007/s12210-023-01184-y](https://doi.org/10.1007/s12210-023-01184-y)
- Peter, K., Pätzold, M., Molina-Cuberos, G., et al. 2014, *Icarus*, 233, 66, doi: <https://doi.org/10.1016/j.icarus.2014.01.028>
- Rottman, G. 2005, *SoPh*, 230, 7, doi: [10.1007/s11207-005-8112-6](https://doi.org/10.1007/s11207-005-8112-6)
- Roy, S., Prasad, A., Ghosh, K., Panja, S. C., & Patra, S. N. 2021, *Geomagnetism and Aeronomy*, 61, 128, doi: [10.1134/S0016793221010138](https://doi.org/10.1134/S0016793221010138)
- Shapiro, A. I., Solanki, S. K., Krivova, N. A., et al. 2017, *Nature Astronomy*, 1, 612, doi: [10.1038/s41550-017-0217-y](https://doi.org/10.1038/s41550-017-0217-y)
- Snow, M., Machol, J., Viereck, R., et al. 2019, *Earth and Space Science*, 6, 2106, doi: [10.1029/2019EA000652](https://doi.org/10.1029/2019EA000652)
- Snow, M., McClintock, W. E., Woods, T. N., & Elliott, J. P. 2022, *SoPh*, 297, 55, doi: [10.1007/s11207-022-01984-9](https://doi.org/10.1007/s11207-022-01984-9)
- Snow, M., McClintock, W. E., Woods, T. N., et al. 2005, *SoPh*, 230, 325, doi: [10.1007/s11207-005-6879-0](https://doi.org/10.1007/s11207-005-6879-0)
- Solanki, S. K., Krivova, N. A., & Haigh, J. D. 2013, *ARA&A*, 51, 311, doi: [10.1146/annurev-astro-082812-141007](https://doi.org/10.1146/annurev-astro-082812-141007)
- Solanki, S. K., Schüssler, M., & Fligge, M. 2000, *Nature*, 408, 445, doi: [10.1038/35044027](https://doi.org/10.1038/35044027)
- . 2002, *A&A*, 383, 706, doi: [10.1051/0004-6361:20011790](https://doi.org/10.1051/0004-6361:20011790)
- Sowmya, K., Shapiro, A. I., Rouppe van der Voort, L. H. M., Krivova, N. A., & Solanki, S. K. 2023, *ApJL*, 956, L10, doi: [10.3847/2041-8213/acf92a](https://doi.org/10.3847/2041-8213/acf92a)
- Sowmya, K., Shapiro, A. I., Witzke, V., et al. 2021, *ApJ*, 914, 21, doi: [10.3847/1538-4357/abf247](https://doi.org/10.3847/1538-4357/abf247)
- Tagirov, R. V., Shapiro, A. I., Krivova, N. A., et al. 2019, *A&A*, 631, A178, doi: [10.1051/0004-6361/201935121](https://doi.org/10.1051/0004-6361/201935121)
- Tebabal, A., Damtie, B., Nigussie, M., & Yizengaw, E. 2017, *SoPh*, 292, 112, doi: [10.1007/s11207-017-1128-x](https://doi.org/10.1007/s11207-017-1128-x)
- Thuillier, G., & Bruinsma, S. 2001, *Annales Geophysicae*, 19, 219, doi: [10.5194/angeo-19-219-2001](https://doi.org/10.5194/angeo-19-219-2001)
- Thuillier, G., DeLand, M., Shapiro, A., et al. 2012, *SoPh*, 277, 245, doi: [10.1007/s11207-011-9912-5](https://doi.org/10.1007/s11207-011-9912-5)
- Uitenbroek, H. 1997, *SoPh*, 172, 109, doi: [10.1023/A:1004981412889](https://doi.org/10.1023/A:1004981412889)
- . 2001, *ApJ*, 557, 389, doi: [10.1086/321659](https://doi.org/10.1086/321659)
- Unruh, Y. C., Krivova, N. A., Solanki, S. K., Harder, J. W., & Kopp, G. 2008, *A&A*, 486, 311, doi: [10.1051/0004-6361:20078421](https://doi.org/10.1051/0004-6361:20078421)
- Unruh, Y. C., Solanki, S. K., & Fligge, M. 1999, *A&A*, 345, 635
- Vernazza, J. E., Avrett, E. H., & Loeser, R. 1981, *ApJS*, 45, 635, doi: [10.1086/190731](https://doi.org/10.1086/190731)
- Vieira, L. E. A., & Solanki, S. K. 2010, *A&A*, 509, A100, doi: [10.1051/0004-6361/200913276](https://doi.org/10.1051/0004-6361/200913276)
- Viereck, R., Puga, L., McMullin, D., et al. 2001, *Geophys. Res. Lett.*, 28, 1343, doi: [10.1029/2000GL012551](https://doi.org/10.1029/2000GL012551)
- Viereck, R. A., & Puga, L. C. 1999, *J. Geophys. Res.*, 104, 9995, doi: [10.1029/1998JA900163](https://doi.org/10.1029/1998JA900163)
- Woods, T. N., Harder, J. W., Kopp, G., et al. 2021, *SoPh*, 296, 127, doi: [10.1007/s11207-021-01869-3](https://doi.org/10.1007/s11207-021-01869-3)
- Wu, C. J., Krivova, N. A., Solanki, S. K., & Usoskin, I. G. 2018, *A&A*, 620, A120, doi: [10.1051/0004-6361/201832956](https://doi.org/10.1051/0004-6361/201832956)
- Yeo, K. L., Krivova, N. A., Solanki, S. K., & Glassmeier, K. H. 2014, *A&A*, 570, A85, doi: [10.1051/0004-6361/201423628](https://doi.org/10.1051/0004-6361/201423628)
- Yeo, K. L., Solanki, S. K., Norris, C. M., et al. 2017, *PhRvL*, 119, 9.1102, doi: [10.1103/PhysRevLett.119.091102](https://doi.org/10.1103/PhysRevLett.119.091102)